energies

MDPI

Article

Salt Ion Diffusion Behavior and Adsorption Characteristics of Fracturing Fluid in Tight Sandstone Gas Reservoir

Xueping Zhang [1,2,*], Youquan Liu [1,2], Yuzhou Liu [3], Chuanrong Zhong [4] and Pengfei Zhang [1,2]

[1] Research Institute of Natural Gas Technology, PetroChina Southwest Oil & Gas Field Company, Chengdu 610213, China
[2] Shale Gas Evaluation and Exploitation Key Laboratory of Sichuan Province, Chengdu 610213, China
[3] Development Department, PetroChina Southwest Oil & Gas Field Company, Chengdu 610066, China
[4] College of Energy, Chengdu University of Technology, Chengdu 610059, China
* Correspondence: zhangxp_1992@sina.com

Abstract: The degree of salinity in the hydraulic fracturing rejection fluid of the Shaximiao reservoir in the central Sichuan Basin is high, and the underlying mechanism causing this salinity is not clearly understood. We evaluated the rock structure of tight sandstone, including rock composition, pore structure, ion diffusion, and adsorption behavior, to determine how the rock structure influences the mechanism of the sandstone's interaction with the fracturing fluid. X-ray diffraction revealed that the rock mineral fraction has a significant clay mineral concentration. The results of linear swelling experiments revealed that the water sensitivity of tight sandstone reservoirs exhibits moderately robust characteristics. The time required for salt ion diffusion stabilization is much longer than that required for self-imbibition stabilization, and the diffusion of salt ions is almost log-linear with time after imbibition stabilization. The diffusion rates of salt ions were determined for different single minerals and particle sizes, with clay minerals and particle sizes controlling the diffusion rates. The samples were treated with different concentrations of KCl and acrylamide polymer solutions, and both the pore size distribution and pore throat properties were characterized by low-temperature nitrogen adsorption. Although the adsorption isotherms of both KCl and polymers are consistent with the Langmuir model, their adsorption mechanisms acting on tight sandstone and the effect of adsorption on the pore throat structure are inconsistent. The adsorption of potassium chloride enhances the rock's pore throat diameter and permeability by increasing the uniformity of the pore throat by electrostatic adsorption with clay particles. However, polymer adsorption reduces the pore diameter of the rock and forms a thin film that obstructs the pore throat, complicating the pore throat and weakening its permeability. This research has led to a greater comprehension of the ion diffusion characteristics of the tight sandstone in the Shaximiao reservoir and the adsorption mechanism on the pore structure of the rock.

Keywords: absorption; fractal dimension; ion diffusion; pore throat; tight sandstones

Citation: Zhang, X.; Liu, Y.; Liu, Y.; Zhong, C.; Zhang, P. Salt Ion Diffusion Behavior and Adsorption Characteristics of Fracturing Fluid in Tight Sandstone Gas Reservoir. *Energies* **2023**, *16*, 2877. https://doi.org/10.3390/en16062877

Academic Editor: Dameng Liu

Received: 6 January 2023
Revised: 12 February 2023
Accepted: 16 February 2023
Published: 21 March 2023

1. Introduction

Tight gas is one of the key areas for the exploration and production of unconventional natural gas. Tight gas refers to natural gas produced in sandstone reservoirs with exceptionally low porosity and permeability [1,2]. The high degree of heterogeneity of tight gas reservoirs and the relatively small size of the effective sand body present challenges in the development of these resources. China possesses substantial tight gas reserves. There is significant potential for increasing reserves and tight gas production, which would enhance China's natural gas self-sufficiency. Accelerating the development and utilization of tight gas resources will play a crucial role in assuring China's overall national energy security and its ability to achieve its "dual carbon" goal [3].

With the evolution of horizontal well drilling and fracturing technologies, horizontal wells can now undergo multistage fracturing. Due to the vast fracture network generated

by this procedure, oil and gas production from such multi-fractured wells has grown significantly; this has enabled the development of substantial oil and gas resources in hitherto unexplored tight unconventional reservoirs that are economically viable [4–7]. Since slickwater has the advantages of adjustable viscosity and a relatively low cost, variable viscosity slickwater has steadily become the most widely used fluid for fracturing tight sandstone reservoirs [8–10]. Clay minerals are an essential component of the majority of sandstone reservoirs and are composed of different silicate minerals. Since the surfaces of clays are negatively charged, their contact with the fluid creates an ion exchange effect by acting as a cation exchanger [11]. When water is injected into subsurface formations, fine particles expand and migrate with the flowing fluid, resulting in pore obstruction and a decrease in permeability, which decreases the volume of fluid that can be injected into the well and the output capacity of the well [12,13]. Particle migration is mainly controlled by factors such as salt concentration, the type of clay in the rock, ion exchange, and temperature [14].

The formation mechanism of high-salinity flowback drainage has attracted considerable attention due to the increasing demand for cost reduction and efficiency improvement in unconventional reservoir reconstruction and the increasingly prominent problem of ineffective recycling of flowback fluid in tight sandstone gas development [15–17]. It is believed that the increase in salinity of the flowback fluid is caused by the dissolution of rock minerals and the transport of salt ions [18]. The complexity of the fracture network can be described by the salinity curve features during the flowback process. The more complicated and dendritic the fracture, the greater the shift in salinity with water recovery from the rejection fluid [19]. Salt ion diffusion behavior out of shale, which is primarily governed by the clay content, TOC, pore volume, and specific surface area, continues to occur in the imbibition fluid medium as imbibition eventually stabilizes [20].

The ion diffusion phenomenon is closely related to imbibition, while the hydration of clay minerals, pore-permeability characteristics, and salt ion adsorption also affect the migration of ions in tight sandstone, making it challenging to reveal the ion diffusion mechanism in tight sandstone. However, there are few studies on the variation in the salinity of fracture rejection fluid, and the diffusion ability of different types of salt ions is not clear. In addition, the structural properties of tight sandstone are relatively complex, making it challenging to directly apply the water–salt transport theory to analyze the ion diffusion in tight sandstone. Therefore, in this work, the tight sandstone gas reservoir of the Shaximiao Formation in the central Sichuan Basin was selected as the subject of experimental investigation. To understand the influence of the rock structure on salt ion diffusion behavior and fracturing fluid adsorption, rock components, pore structure, spontaneous percolation and salt ion diffusion, clay stabilization, and polymer adsorption were investigated. The pore structure was microscopically characterized by low-temperature nitrogen adsorption. The fractal characteristics of the pore structure before and after adsorption were investigated using the Frenkel–Halsey–Hill (FHH) method. This work is beneficial to the improved comprehension of the rock structure of tight sandstone and its effect on salt ion diffusion and fracturing fluid adsorption within the formation.

2. Experiment

2.1. Experimental Equipment and Materials

The tight sandstone samples discussed in this study come from the Jurassic Shaximiao Formation in the Sichuan Basin and include both field-drilled rock and crushed core. The tight gas reservoir of the Shaximiao Formation in central Sichuan mainly develops deltaic plain-frontal deposits with obvious braided river delta characteristics. Longitudinally, it develops multi-phase river sand with large cumulative thickness and a stacked contiguous distribution. The river sand reservoir is characterized by the low porosity (average porosity 11.3%) and low permeability (average permeability 0.45 mD) of a tight sandstone reservoir. The reservoir temperature ranges from 66 to 73 °C, and the formation pressure ranges from 19.1 to 24.5 MPa, which is a normal temperature and pressure for a gas reservoir. The

experimental evaluation apparatus and schematic diagram for imbibition, ion diffusion, and adsorption properties are outlined in Figure 1.

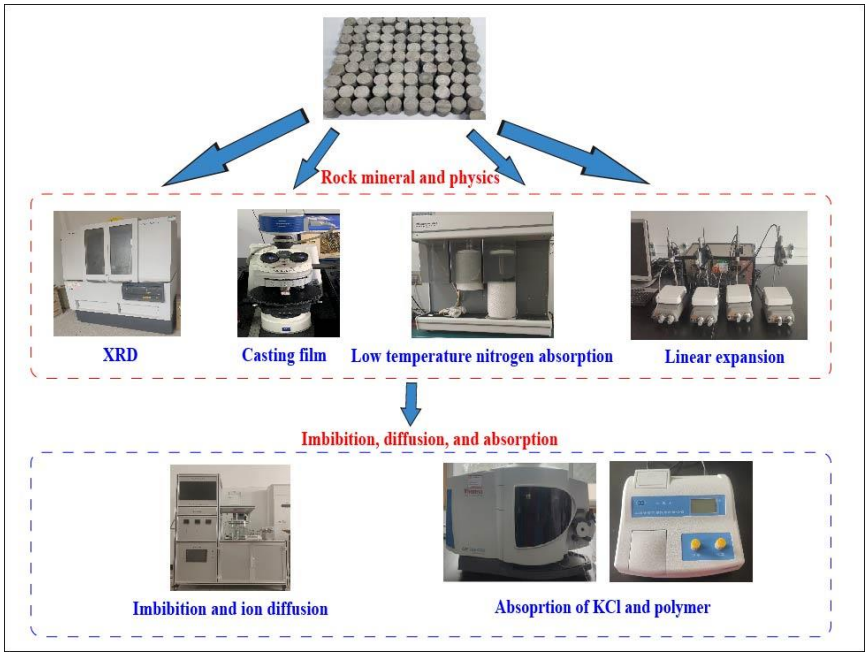

Figure 1. Experimental evaluation apparatus and schematic diagram for imbibition, ion diffusion, and adsorption properties.

The whole rock and clay mineral content were measured using an X-ray diffractometer (XPert3Powder), which showed that the tight sandstone samples had relatively high quartz content, as shown in Table 1. A transmission polarized light microscope (IEISS Axio Imager A_2) was used to analyze rock materials using cast thin sections. The lithology of the sample is composed primarily of fine-grained and medium-fine-grained rock chip feldspathic sandstone, as seen in Figure 2. The intergrain is cemented with a chlorite liner and calcite plates. Effective storage space is dominated by residual primary intergranular pores and corrosion is severe. The ASAP 2020 plus HD88 fully automatic gas adsorption instrument, supplied by McMurray-Tick (Shanghai) Instruments Co., Ltd. (Shanghai, China), was used for low-temperature nitrogen adsorption measurement to characterize the specific surface and pore size distribution of rock samples.

Table 1. Mineral content (w_t%) of the sandstone samples determined by XRD.

Mass Fraction of Mineral						Mass Fraction of Clay Mineral			
Quartz	**Orthoclase**	**Plagioclase**	**Calcite**	**Pyrite**	**Clay**	**Illite/Smectite**	**Illite**	**Kaolinite**	**Chlorite**
33.6	4.1	22.0	2.2	0.7	37.5	29	43	27	1

2.2. Experimental Procedures

2.2.1. Imbibition Experiment

To determine the imbibition behavior of sandstone samples, a full-scale spontaneous imbibition experiment was conducted with deionized water as the imbibition fluid and a Mettler balance to precisely quantify the weight of the sample during imbibition. A data cable connected the scale to a computer to record the imbibition mass over time. Prior to the testing, standard cylinders of 5 cm in length and 2.5 cm in diameter were cut and pre-dried in an oven at 120 °C for 24 h.

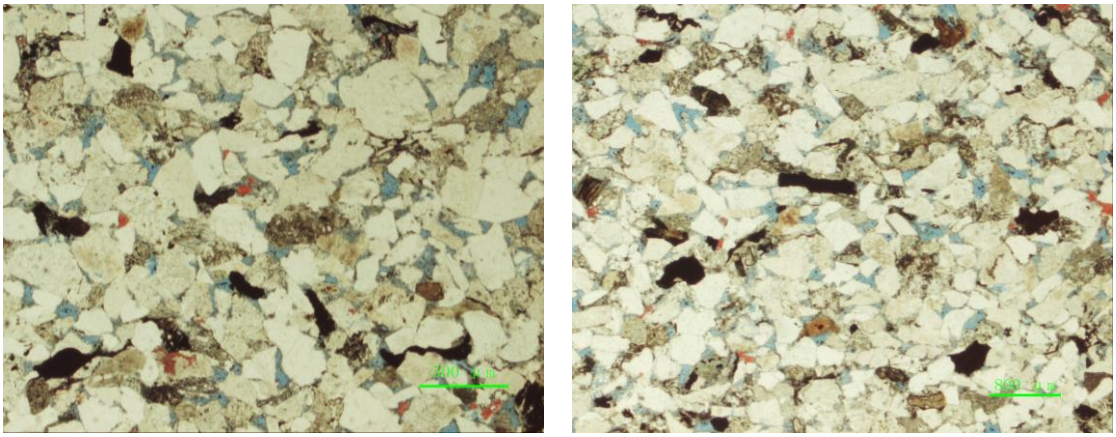

(**a**) (**b**)

Figure 2. Images of cast body thin section analysis of tight sandstone gas reservoir samples. (**a**) medium-grained rock chips. (**b**) medium-fine-grained rock chips.

2.2.2. Salt Ion Diffusion

Salt ion diffusion experiments were conducted using a Mettler SevenExcellence multi-parameter conductivity meter. A mortar and a sieve were used to obtain particle samples with varying mesh sizes. For the experiments, 10 g of the sample and 200 mL of deionized water combined in a sealed glass flask. At regular intervals, the lid of the sealed flask was removed, and the conductivity of the liquid was measured with an electrode, after which the flask was resealed. The test conditions were fixed at 25 °C and atmospheric pressure.

2.2.3. Isothermal Adsorption Experiment

Due to its easy availability and anti-swelling properties, KCl is a widely used clay stabilizer for the hydraulic fracturing of oil and gas reservoirs [21]. Potassium chloride was selected as the adsorbent and deionized water was used as the adsorbent solvent to carry out isothermal adsorption experiments on tight sandstone powder samples of different particle sizes at 25 °C. Four different concentrations of potassium chloride solutions were prepared and mixed in 250 mL sealed glass vials for each rock sample. The isothermal adsorption experiments were carried out in a constant temperature water bath, and the samples were centrifuged at regular intervals to obtain the supernatant for chemical analysis. The extracted supernatant was diluted and fixed volume. Subsequently, the potassium ion content was determined using inductively coupled plasma-optical emission spectrometry (ICP-OES), with iCAP7400 supplied by Thermo Fisher Scientific Co., Ltd., Waltham, MA, USA.

As the most prevalent resistance reducer for hydraulic fracturing, modified polyacrylamide is the most prominent formulation of fracturing fluid for production enhancement and stabilization work in unconventional oil and gas reservoirs [22]. In this work, modified polyacrylamide resistance reducer produced by Chengdu Nengte Technology Co., Ltd. (Chengdu, China), were used to prepare polymer solutions of different concentrations for isothermal adsorption experiments at 25 °C. Polymer solution concentration was measured by the turbidity method [23] using a WGZ-800 turbidimeter supplied by Shanghai Xinrui Instruments Co., Ltd. (Shanghai, China).

The adsorption pattern of substances on the surface of sandstone can be quantitatively described using four empirical models of adsorption isotherms. Langmuir first proposed the single-molecular-layer adsorption model in 1916; the adsorption equation was derived from the adsorption kinetics point of view [24], as depicted in Equation (1). Freundlich et al. (1906) summarized the empirical equation for Freundlich adsorption from extensive experimental data [25], as shown in Equation (2). The Termkin isotherm model is usually

expressed in the form of a linear equation [26], as shown in Equation (3). The simplest isotherm model is the linear isotherm model [27], which is expressed in linear Equation (4):

$$q_e = \frac{q_0 K_{ad} C_e}{1 + K_{ad} C_e} \quad (1)$$

$$q_f = K_f C_e^{1/n} \quad (2)$$

$$q_e = B\mathrm{In}K_t + B\mathrm{In}C_e \quad (3)$$

$$q_e = K_H C_e + C \quad (4)$$

where q_0 and K_{ad} are Langmuir adsorption isotherm constants; n and K_f are Freundlich adsorption isotherm constants; B and K_t are Termkin adsorption isotherm constants; C and K_H are linear adsorption isotherm constants; Ce denotes equilibrium concentration, mg/L; and q_e represents equilibrium adsorption amount, mg/g-rock.

2.2.4. Low-Temperature Liquid Nitrogen Adsorption Experiment

The rock samples used in the experiment are from the Shaximiao Formation reservoir. The experimental instrument was the specific surface area and pore size analyzer produced by Bester Company. Rock samples with different particle sizes were selected and subjected to nitrogen adsorption at a temperature of 77 K and purity of 99%. The experimental steps are as follows: (1) A certain amount of the rock sample was selected, crushed, and placed in the analyzer. The particle size was 0.250–0.425 mm, and the mass was about 2.5 g. (2) The samples were then put into the degassing tube, the temperature was raised to 120 °C, and the tube was subject to vacuum for 8 h. (3) The samples were backfilled with nitrogen gas, the temperature was kept constant, and the partial pressure of nitrogen gas was first slowly raised and then gradually reduced; the duration of the experiment was about 5 h. Finally, the specific surface area, pore size, and pore volume distribution of the rock samples were measured and counted based on the liquid nitrogen adsorption data. The pore size distribution was calculated.

3. Results and Discussion

3.1. Analysis of Pore Throat Characteristics

Low-temperature nitrogen adsorption was used to characterize the pore throat characteristics of tight sandstone before and after treatment with different fluids, including key parameters such as specific surface, pore volume, and average pore size, which are shown in Table 2. The initial specific area of the tight sandstone sample was 3.6813 m^2/g. After treating the rock sample with 0.01%, 0.02%, 0.04%, 0.08%, 0.10%, and 0.20% acrylamide polymer reagent in turn, the specific surface and pore volume were found to gradually increase with the increase in the polymer concentration. Meanwhile, the average pore size decreased continuously with the increase in polymer concentration. However, when the tight sandstone samples were treated with different concentrations of KCl, the specific surface and pore volume increased and then decreased with the increase in the KCl concentration. Correspondingly, the average pore size showed the opposite variation.

Table 2. The pore structure of sample.

Treatment Agents	Specific Surface Area, m^2/g	Pore Volume, cc/g	Average Pore Diameter/nm
untreated	3.6813	0.006186	8.4016
0.01% polymer	3.9676	0.006965	8.2525
0.02% polymer	4.9385	0.007798	7.3704
0.04% polymer	5.3832	0.008186	6.4060
0.08% polymer	6.4341	0.009594	6.3157
0.1% polymer	6.8269	0.010933	5.9642

Table 2. *Cont.*

Treatment Agents	Specific Surface Area, m^2/g	Pore Volume, cc/g	Average Pore Diameter/nm
0.2% polymer	7.0832	0.009919	5.6307
1% KCl	6.0224	0.008263	5.4883
2% KCl	2.7416	0.004384	6.3966
5% KCl	1.6359	0.004102	10.0309
10%KCl	1.0640	0.003067	11.5280

The low-temperature nitrogen adsorption–desorption curves of tight sandstone treated with polymer and KCl are plotted in Figures 3a and 3b, respectively. The pore throat distribution when treated with polymer and KCl are presented in Figures 4a and 4b, respectively. As the mass concentration of the polymer solution increases, the capillary pressure curves in Figure 3a line up from the lower to the upper sections of the graph. This indicates that, with regard to polymer adsorption, the permeability of the rock pores decreases with the increase in the polymer mass concentration. The capillary pressure curve in Figure 3b decreases from the top of the graph to the bottom as the mass concentration of the KCl solution increases. The results indicate that the permeability of the rock pores increases with the increase in the mass concentration of KCl after the adsorption of KCl. It can be seen from Figure 4a that, on the one hand, in the 10–100 nm pore diameter range, the volume of pores decreases as the mass concentration of the polymer solution increases. On the other hand, in the 1–10 nm pore diameter range, the volume of the pores increases rapidly with the increase in pore diameter. This indicates that when the polymer solution flows in porous media, the retention of polymer molecules in the pores of the rock causes a reduction in the pore flow channels, which is due to the rheological properties of the reagent solution–rock pore system, as well as the adsorption and hysteresis involved, which are quite different from systems where general aqueous solutions have been used. As the mass concentration of the polymer solution increases, the retention of the polymer in large pores increases, making the pore radius smaller and resulting in the originally larger pore channels becoming smaller at the next level. Thus, as the mass concentration of the polymer solution increases, the pore volume of the large pore channels decreases and then begins to increase for the smaller pore channels at the next level. The results in Figure 4b show that the pores in the 1–10 nm pore size range keep decreasing with the increase in the concentration of adsorbent KCl, while the pore distribution in the 10–100 nm range becomes wider. This can be attributed to the adsorption of KCl on the surface of clay minerals, which prevents these minerals from undergoing swelling due to hydration, and in turn results in an increased average pore size and makes the rock matrix more permeable. According to the water–sensitive mechanism of clay particles, the additive system causes agglomeration within the minerals as well as mutual resistance, thus preventing their dispersion and transfer. The KCl clay stabilizer is added to the injected water and creates a water–repellent surface on the surface of the clay resulting from the interaction between the surface of the clay crystal layer and its positive ions. This prevents the clay from swelling via hydration and weakens the mutual attraction between the dipoles in the molecular bonds and the water molecules, thus reducing the sensitivity of the clay minerals to damage.

3.2. Fractal Dimension Analysis

Fractal theory was first proposed by French mathematician Mandelbrot in 1975 [28]. It is used to describe the structural characteristics of complex objects in nature and is now widely used in the prediction of a reservoir's fracture, pore structure, and heterogeneity. The fractal characteristics of rock are determined by its pore structure and irregularity, and the fractal dimension D can quantitatively characterize the irregularity of the pore structure and roughness of the surface [29]. Pore image data, nitrogen gas adsorption data, mercury injection flow test data, and nuclear magnetic resonance test data can be used to study the fractal characteristics of reservoir pores [30,31]. In view of the reservoir

space of different types of sandstone, researchers have tried to carry out fractal studies using different models such as the Frenkel–Halsey–Hill (FHH), NK (Newton–Kantorovich), and Neimark methods [32–35]. In this work, we calculated the fractal dimensions of tight sandstone before and after adsorption using the most commonly used FHH model [29] and based on the data from the low-temperature nitrogen adsorption experiment. The FHH fractal dimension model is defined as the following Equation (5):

$$\mathrm{In}V = (D-3)\mathrm{In}\left[\mathrm{In}\left(\frac{P_0}{P}\right)\right] + \mathrm{C} \tag{5}$$

where V is the nitrogen adsorption amount when the equilibrium pressure is P, m^3/g; D stands for the fractal dimension; P_0 represents the pressure when the gas is adsorbed and saturated, MPa; and C is a constant.

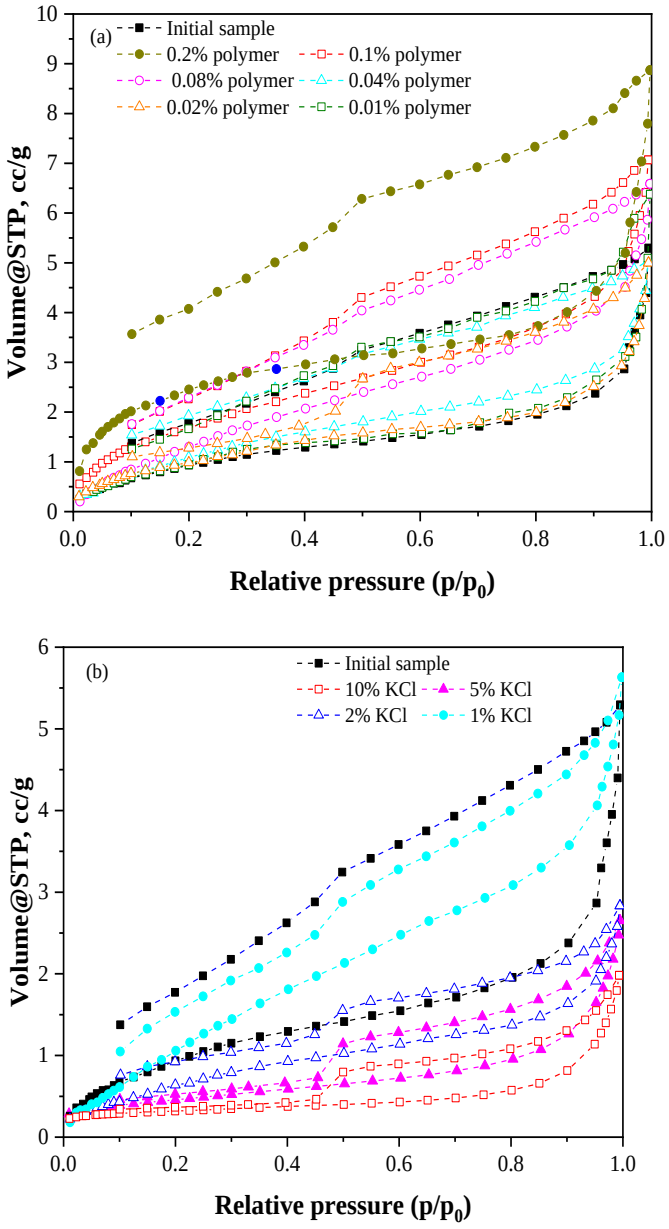

Figure 3. Low-temperature nitrogen adsorption–desorption curves of tight sandstone: (**a**) polymer and (**b**) KCl.

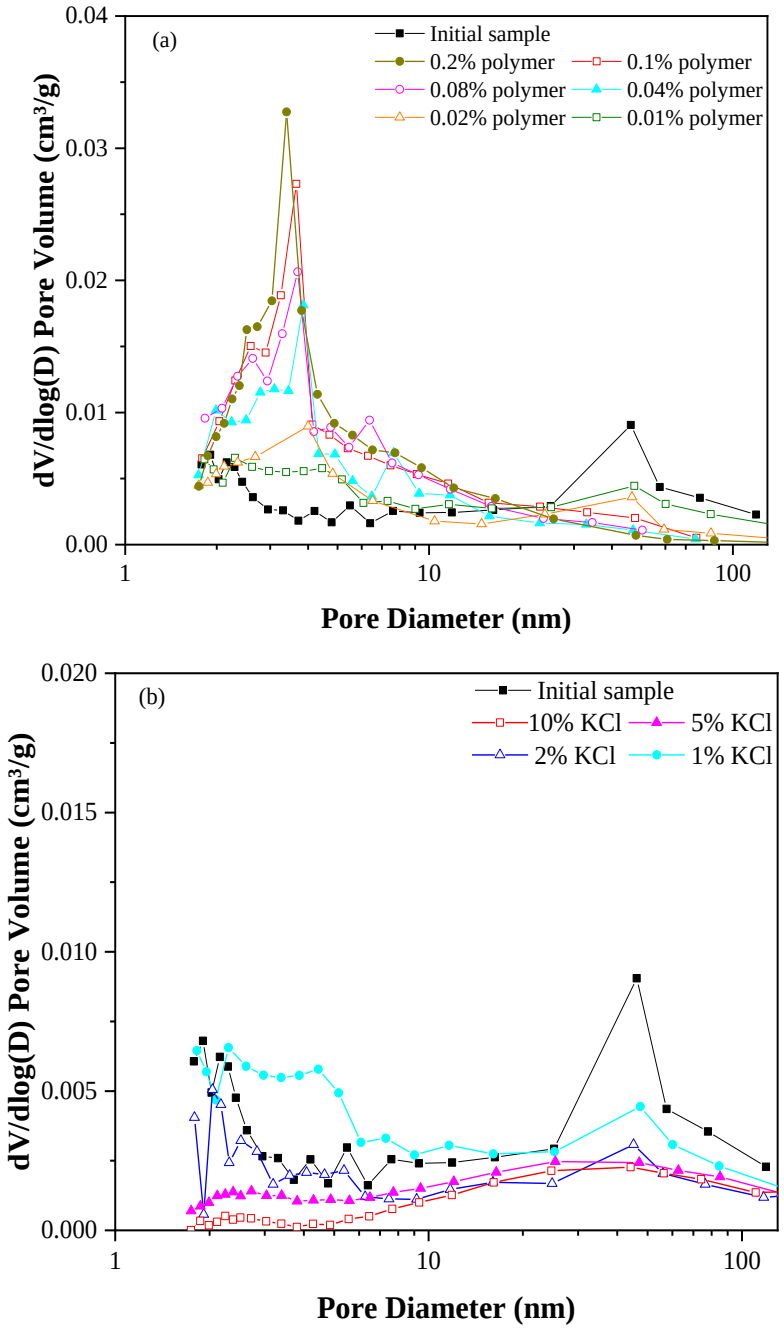

Figure 4. Pore throat distribution of tight sandstone: (**a**) polymer and (**b**) KCl.

The fractal dimensions of tight sandstone derived from the fractal FHH model are listed in Table 3. The relationship between ln(V) and ln(ln (P_0/P)) according to the fractal FHH equation is plotted in Figure 5. The curve is clearly divided into two segments by P_0/P = 0.5 for segmental fitting. At lower relative pressure, D_1, which represents the fractal dimension of the surface, is closely related to the van der Waals force. At a higher relative pressure, the fractal dimension D_2, representing the pore structure, is closely related to the capillary condensation behavior. As the polymer concentration increases, the fractal dimension D_2 also shows an increasing trend, indicating that polymer adsorption makes the pore throat structure of dense sandstone more complex and less homogeneous, which is the main reason for the decrease in permeability. However, as the KCl concentration increases, the fractal dimension D_2 becomes smaller, indicating that KCl adsorption makes the pore throat structure of tight sandstone more homogeneous and uniform, which improves the permeability of the reservoir. The flat surface and uniform pore throat of the particles,

which result from the salt solution treatment, are mainly due to the strong electrostatic interaction between the positively charged ions and the negatively charged clay, which results in a strong van der Waals force between the clay's crystal layers, in turn leading to the firm adsorption of the clay crystal layers and the formation of a dense clay layer.

Table 3. The fractal dimension of tight sandstone derived from the fractal FHH model.

Sample	$P/P_0 < 0.5$			$P/P_0 > 0.5$		
	Fitting Equation	R^2	D_1	Fitting Equation	R^2	D_2
Initial sample	y = −0.9772x + 0.2981	0.9549	2.0228	y = −0.2723x + 0.5604	0.9946	2.7277
0.01% polymer	y = −0.9788x + 0.3573	0.9634	2.0212	y = −0.2636x + 0.3120	0.9963	2.7364
0.02% polymer	y = −1.0645x + 0.5021	0.9643	1.9355	y = −0.2461x + 0.3518	0.9973	2.7539
0.04% polymer	y = −1.1492x + 0.5356	0.9398	1.8508	y = −0.2117x + 0.5604	0.9943	2.7883
0.08% polymer	y = −1.2976x + 0.7831	0.9459	1.7024	y = −0.1831x + 0.9152	0.9612	2.8169
0.1% polymer	y = −0.8536x + 0.8825	0.9608	2.1464	y = −0.2007x + 0.9778	0.9873	2.7993
0.2% polymer	y = −0.6497x + 1.1454	0.8841	2.3503	y = −0.2025x + 1.0445	0.9841	2.7975
1% KCl	y = −1.3704x + 0.6019	0.9754	1.6296	y = −0.1681x + 0.8321	0.9407	2.8319
2% KCl	y = −0.8895x − 0.0944	0.9875	2.1105	y = −0.2128x − 0.0042	0.9905	2.7872
5% KCl	y = −0.4424x − 0.5691	0.9997	2.5576	y = −0.3053x − 0.5045	0.9845	2.6947
10% KCl	y = −0.2904x − 1.0023	0.9929	2.7096	y = −0.3834x − 1.0894	0.9874	2.0126

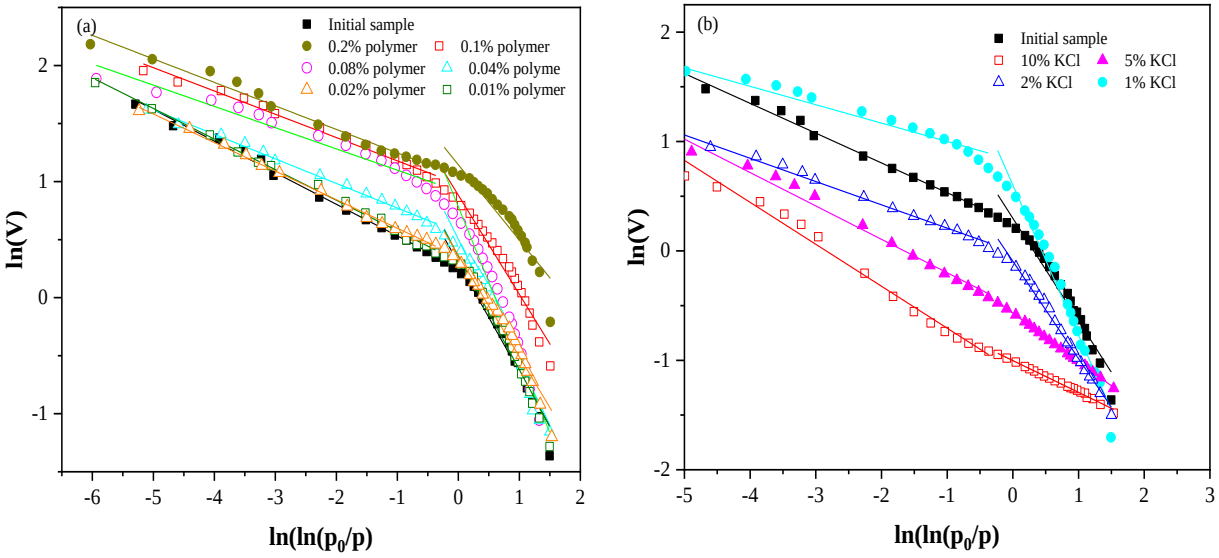

Figure 5. The fractal characteristics of samples based on nitrogen adsorption data: (**a**) polymer and (**b**) KCl.

3.3. Linear Expansion Rate

We used an OFI150–80–1 dynamic linear swell meter to determine the linear swell rate of tight sandstone to evaluate the degree of reservoir water sensitivity. First, 10 g of accurately weighed, crushed, 100 mesh tight sandstone powder was pressed at 20 MPa for 2 h to form a small cylindrical rock sample of approximately 1 cm in height. The prepared sample was placed in a working cylinder, and different experimental fluids were passed into the core cylinder for several sets of experiments. The equipment was run and the samples were fluidized for 24 h with a constant expansion height. The linear expansion rate of the artificial cores in the axial direction was recorded.

The linear swelling rate curves with time for the same tight sandstone sample in different test fluids are shown in Figure 6. The linear swelling rate using deionized water as the working fluid was determined to be 8.74% of the tight sandstone of the Shaximiao reservoir. This reservoir was thus identified as having moderately strong water-sensitive properties, and anti-expansion agents need to be added to the field construction fracturing fluid to prevent water-sensitive damage to the reservoir from clay mineral swelling. Similarly, the linear swelling rates of 0.1% acrylamide polymer and 5% potassium chloride were

evaluated as 6.25% and 3.45%, respectively. Compared with deionized water as the working fluid, the use of 5% potassium chloride as the working fluid reduced the linear swelling of tight sandstone by 60.53%. Moreover, 0.1% acrylamide polymer reduced it by 28.49%, 1% polyamide reduced it by 88.33%, and 10% potassium chloride reduced it by 89.36%. Compared with potassium chloride, the low concentration of polyamide can significantly inhibit the hydration and swelling of the clay minerals contained in tight sandstone.

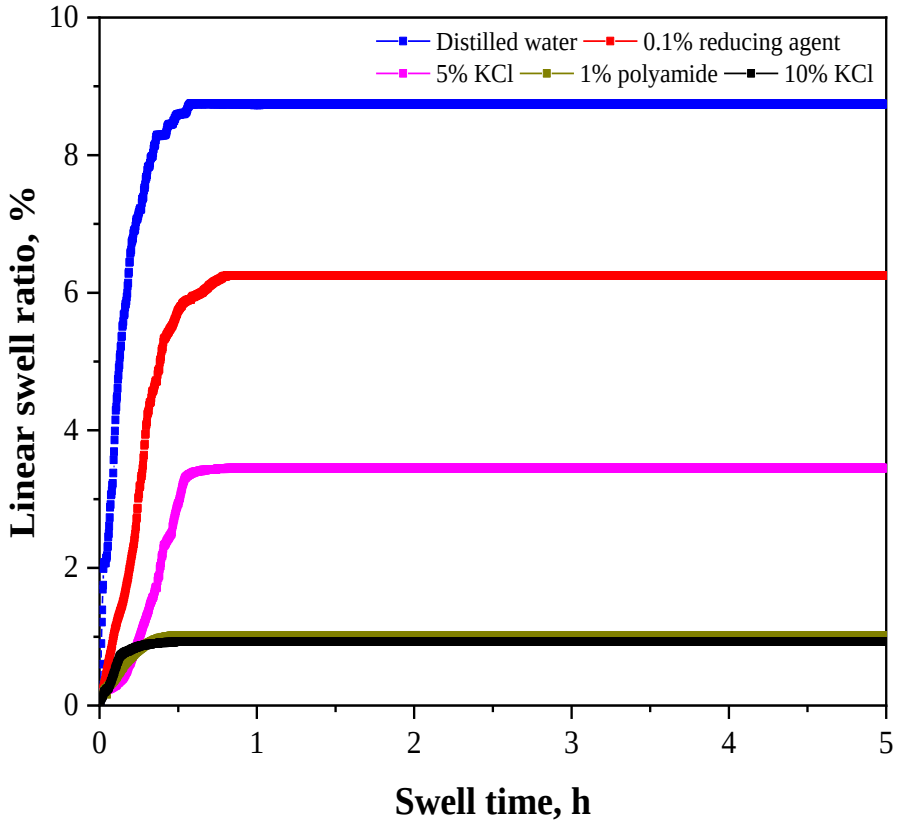

Figure 6. Linear expansion rate of the tight sandstone sample treated with different fluid.

3.4. Imbibition and Ion Diffusion

The basic parameters for ion diffusion in tight sandstone samples with different diameters are listed in Table 4. The results show that smaller particle sizes exhibit greater initial conductivity G_0. At the same time, the small particle size leads to a smaller corresponding ion diffusion rate D. The slope of the microcrack diffusion segment is significantly higher than that of the matrix ion diffusion segment for samples with particle sizes of 0.1 mm and above and exhibits a time index I that is higher than that of time index II, indicating the presence of certain microcracks in the large–size samples. The diffusion of salt ions from tight sandstone reservoirs through the fracturing fluid is the main reason for the high mineralization of the rejection fluid. The salt ion concentration in the rejection fluid can reflect the fracture characteristics of the formation. Spontaneous imbibition and salt ion diffusion experiments were carried out, and the experimental results are shown in Figure 7. Figure 7a depicts the imbibition curve of the plunger sample in deionized water and Figure 7b shows the ion diffusion curve of the corresponding powder sample. In Figure 7c, the lateral coordinate time is depicted logarithmically to compare the imbibition and ion diffusion curve characteristics. The results show that the imbibition reaches stability before the ion diffusion, reaching 50% of the imbibition capacity at 24 h. However, it is difficult for the ion diffusion curve to reach stability, and the conductivity continues to increase after 200 days.

Table 4. Basic parameters for ion diffusion in tight sandstone samples.

Mesh	Diameter, mm	G_0, us/cm	D, (us/cm)/t$^{0.5}$	Time Index I	Time Index II
10	2	28.8	11.6831	0.40	0.18
100	0.15	35.6	9.4232	0.33	0.15
120	0.13	46.2	8.6934	0.25	0.13
150	0.10	60.1	6.3972	0.17	0.13
180	0.08	81.4	6.1970	0.14	0.15
240	0.06	91.6	4.8045	0.10	0.16
280	0.05	109.2	2.3031	0.048	0.18

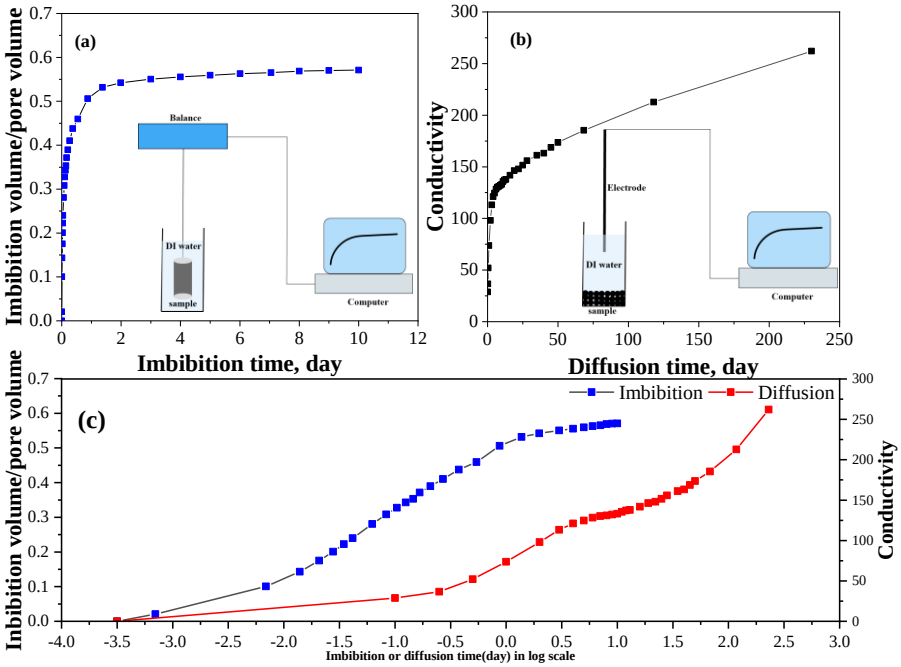

Figure 7. Imbibition and salt ion diffusion curves of sandstone sample.

The tight sandstone of the Shaximiao Formation was processed into powders of different particle sizes: 10 mesh, 100 mesh, 120 mesh, 150 mesh, 180 mesh, 240 mesh, and 280 mesh. Conductivity experiments were carried out by mixing 10 g of the sample with 200 mL of deionized water in a 250 mL sealed glass bottle. Figure 8a,b show the electrical conductivity versus square root of diffusion time and double logarithm at different particle sizes, respectively. Figure 8a depicts the magnitude of the rate of ion diffusion, while Figure 8b reflects the pore connectivity. As shown in Figure 8a, the conductivity curve of tight sandstone particles has a two–stage feature, and the curve turns after around one week of diffusion, indicating that the tight sandstone formation has some microfracture development; however, the scale of the microfracture is small. The higher ion diffusion rate in the initial stage is mainly due to the contribution of microfractures, while the later stage mainly reflects the ion diffusion process of the matrix. As the particle diameter decreases to 0.05 mm, the conductivity curve is approximately a straight line, at which time there are basically no microfractures, reflecting the matrix's ion diffusion properties. The scale of the microfractures in tight sandstone formations varies continuously, and the smaller the particles are, the smaller the scale of microfractures that can exist. The different morphologies of the conductivity curves depend to a large extent on the differences in microscopic pore structure. The crushed tight rocks reflect the characteristics of the matrix, and the complex matrix pore structure of tight rocks leads to the time index not being exactly equal to 0.5. Therefore, different curve patterns are presented under the square root of the time curve.

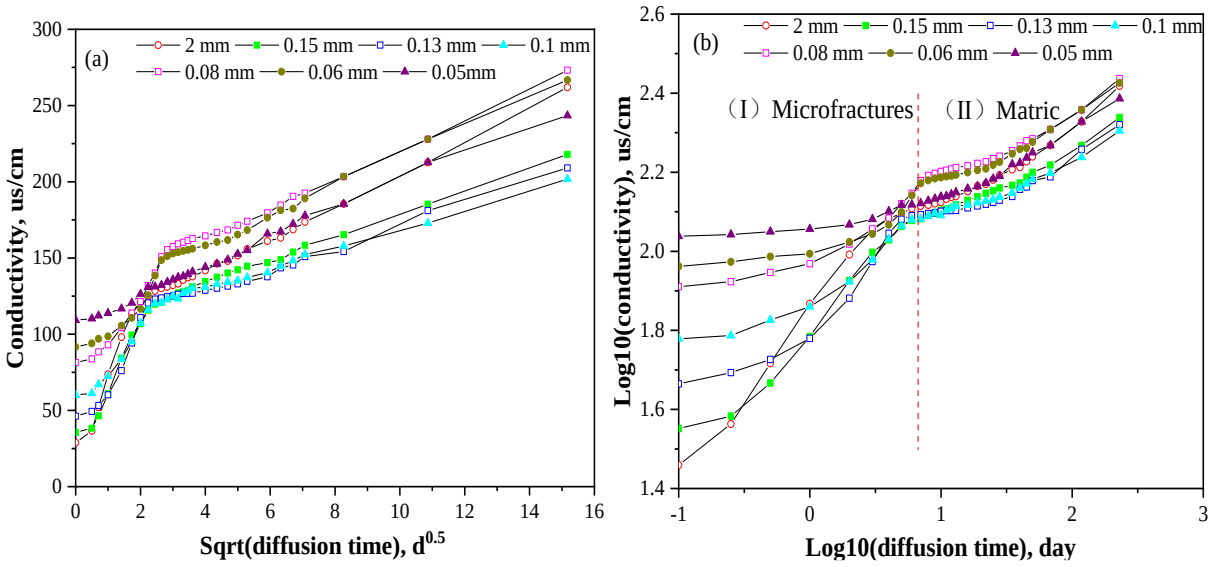

Figure 8. Ion diffusion curves of sandstone sample with different particle sizes: (**a**) conductivity over time$^{0.5}$ and (**b**) double logarithm of conductivity with time.

The ion diffusion curves for single non–clay minerals are presented as conventional and double logarithmic conductivity curves in Figure 9a and 9b, respectively. Meanwhile, the conventional and logarithmic ion diffusion curves for single clay minerals are plotted in Figure 10a and 10b, respectively. The results show that the conductivity of single–component mineral increases with time. However, different minerals have different conductivity profile characteristics. The conductivity stabilization time of non–clay minerals is longer compared to that of clay minerals, and the conductivity continues to increase after more than 200 days of immersion. Salinity analysis of the immersion solution for tight sandstone particles is listed in Table 5. Among the non–clay minerals, pyrite, as the main source of ferrous ions in the rejection solution, has significantly higher conductivity than other minerals, and it has the characteristic of significantly increasing the conductivity of the solution, which is attributed to the very good conductivity of pyrite itself. Among the clay minerals, only kaolinite contributes a little to the conductivity, while illite and montmorillonite make a relatively large contribution to the conductivity. The tight sandstone reservoir has very low pyrite content, so the high clay mineral content is considered to be the important source of high mineralization in the fracturing rejection fluid. The contribution of non–clay minerals to conductivity is 16.9%, while this value is 24.6% for clay minerals, and the remaining 58.5% is attributed to dissolution of soluble salts and carryover of reservoir fluids.

3.5. Isothermal Absorption

The adsorption mechanism of tight sandstone powder in different solution media, including potassium chloride and polymers, is shown schematically in Figure 11. The parameters calculated by the Langmuir, Freundlich, Temkin, and linear adsorption isotherm models are shown in Table 6. The tight sandstone exhibits different mechanisms of adsorption when treated with potassium chloride and polymer. The sandstone reservoir has a negative charge due to the clay–mineral–rich surface. The clay particles attract the cations from the clay surface together by electrostatic attraction [36]. Potassium chloride ionizes large amounts of potassium ions and neutralizes the electronegative ions in the clay, resulting in strong electrostatic adsorption. The polymers mainly form polymer films on the mineral surface, locking the channels of the water molecules.

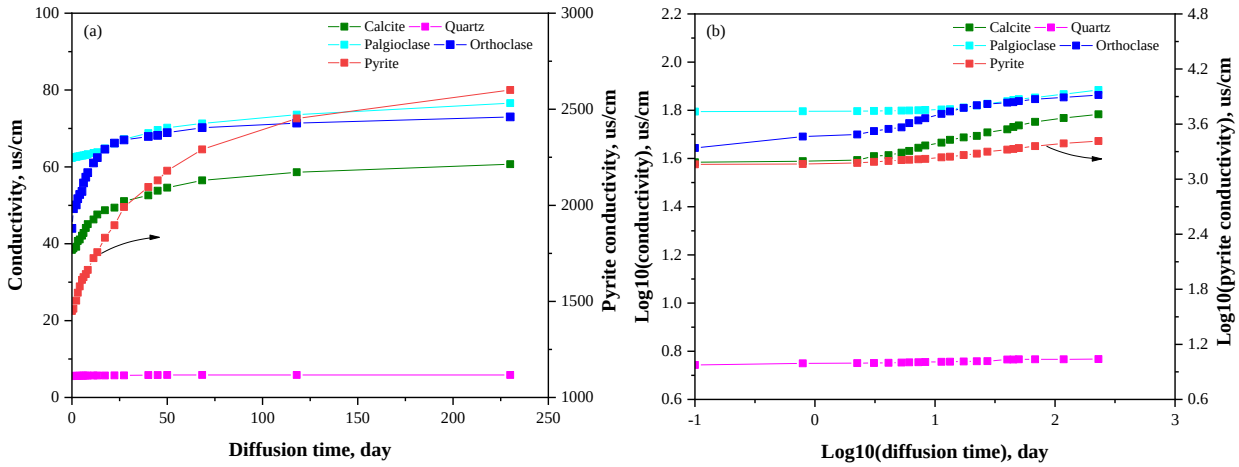

Figure 9. Ion diffusion curves of single non–clay minerasl: (**a**) conductivity over time and (**b**) double logarithm of conductivity with time.

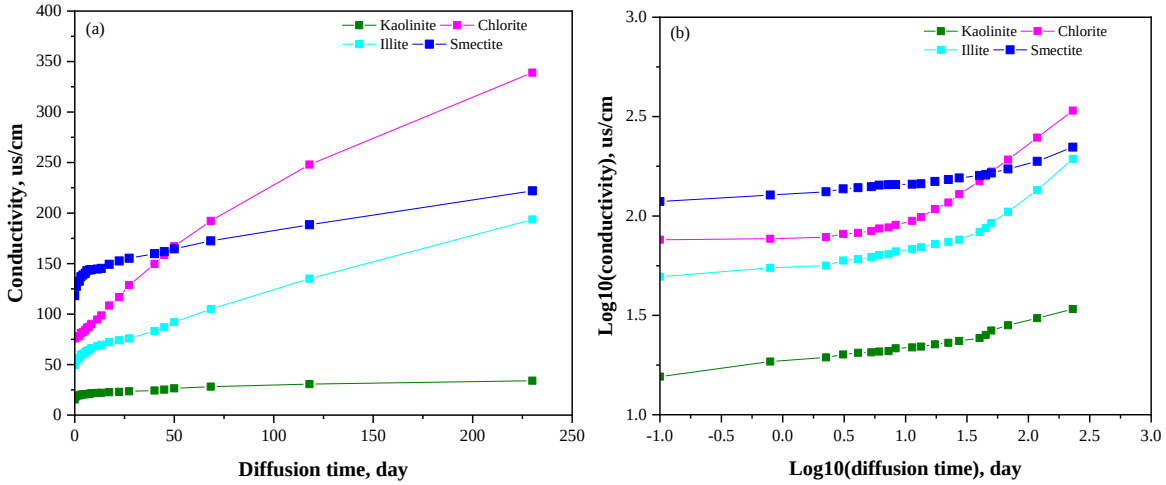

Figure 10. Ion diffusion curves of single clay minerals: (**a**) conductivity over time and (**b**) double logarithm of conductivity with time.

Table 5. Salinity analysis of immersion solution for tight sandstone particles.

	Non–Clay Mineral					Clay Mineral			
	Quartz	**Orthoclase**	**Plagioclase**	**Calcite**	**Pyrite**	**Illite/Smectite**	**Illite**	**Kaolinite**	**Chlorite**
Mass fraction, %	33.6	4.1	22.0	2.2	0.7	10.9	16.1	10.1	0.4
Conductivity, us/cm	5.9	73.0	76.6	60.7	2600	222.0	193.6	34.0	339.0
Proportion, %	0.8	1.2	6.9	0.5	7.5	9.9	12.8	1.4	0.5

The adsorption curves of KCl on tight sandstone with time and isothermal adsorption curves are shown in Figure 12a and 12b, respectively. Different concentrations of 1%, 2%, 5%, and 10% KCl were used as adsorption solutions to fully submerge the dense sandstone powder, and the solution concentrations were quantified at different time periods. The adsorption equilibrium time of KCl becomes longer as the concentration increases, and the rate of adsorption decreases with time until the adsorption equilibrium is reached. The maximum adsorption capacity of 81.9397 mg/g for KCl exhibited by tight sandstone powder can be obtained from the adsorption isotherm, and the adsorption characteristics can be interpreted well by the Langmuir model. Based on the measured turbidity data for known polymer concentrations, a standard curve for polymer adsorption was plotted, as detailed in Figure 13. The curve equation y= 4665.57x − 2.39 with a correlation coefficient

of 0·9998 can be derived from the polymer standard curve plot. The concentration of the polymer after adsorption was calculated from the measured turbidity value of the test solution based on the standard curve equation, and this concentration is the equilibrium concentration Ce when the adsorption reaches equilibrium. Acrylamide polymers at mass concentrations of 0.01%, 0.02%, 0.04%, 0.08%, 0.1%, and 0.2% were added to the tight sandstone powder, and the adsorption per unit mass measured at 25 °C in a water bath is shown in Figure 14a. The isothermal adsorption data were fitted to curves using four different adsorption models, as shown in Figure 14b. The amount of adsorption per unit mass of tight sandstone sample gradually increases with increasing polymer concentration. The higher the initial concentration of polymer, the longer it takes to reach the adsorption equilibrium. The maximum adsorption amount reaches 0.6347 mg/g when the polymer concentration is 0.2%, and it takes at least 24 h to reach the adsorption equilibrium at this time. The adsorption of acrylamide polymer on tight sandstone minerals satisfies the Langmuir adsorption law and it has a lower saturation adsorption capacity than KCl.

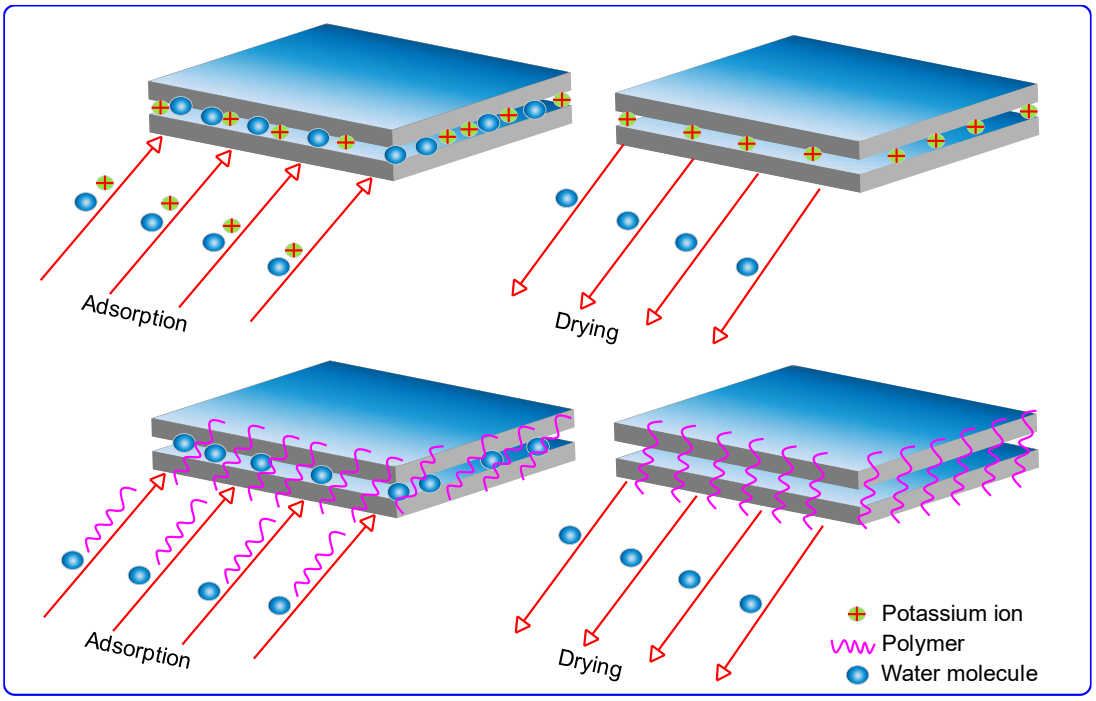

Figure 11. Schematic diagram of adsorption mechanism.

Table 6. Relevant parameters of the adsorption isotherm.

Treated Agent	Isotherm	Fitting Equation	R^2	Parameter	
polymer	Langmuir	$q_e = \frac{1.6420 \times 4.5895 C_e}{1+4.5895 C_e}$	0.9989	$q_{0\,=}$ 1.6420	K_{ad} = 4.5895
	Freundlich	$q_e = 2.9061 C_e^{0.7601}$	0.9988	n = 1.3156	K_f = 2.9061
	Temkin	$q_e = 0.1694 In(C_e) + 0.8672$	0.8845	B = 0.1694	K_t = 167.2016
	Linear	$q_e = 4.4302 C_e + 0.05325$	0.9859	C = 0.05325	K_H = 4.4302
KCl	Langmuir	$q_e = \frac{81.9397 \times 0.1166 C_e}{1+0.1166 C_e}$	0.9999	$q_{0\,=}$ 81.9397	K_{ad} = 0.1166
	Freundlich	$q_e = 9.1249 C_e^{0.7298}$	0.9875	n = 1.3702	K_f = 9.1249
	Temkin	$q_e = 12.0910 In(C_e) + 10.6784$	0.9783	B = 12.0910	K_t = 2.4186
	Linear	$q_e = 5.0542 C_e + 3.6923$	0.9840	C = 3.6923	K_H = 5.0542

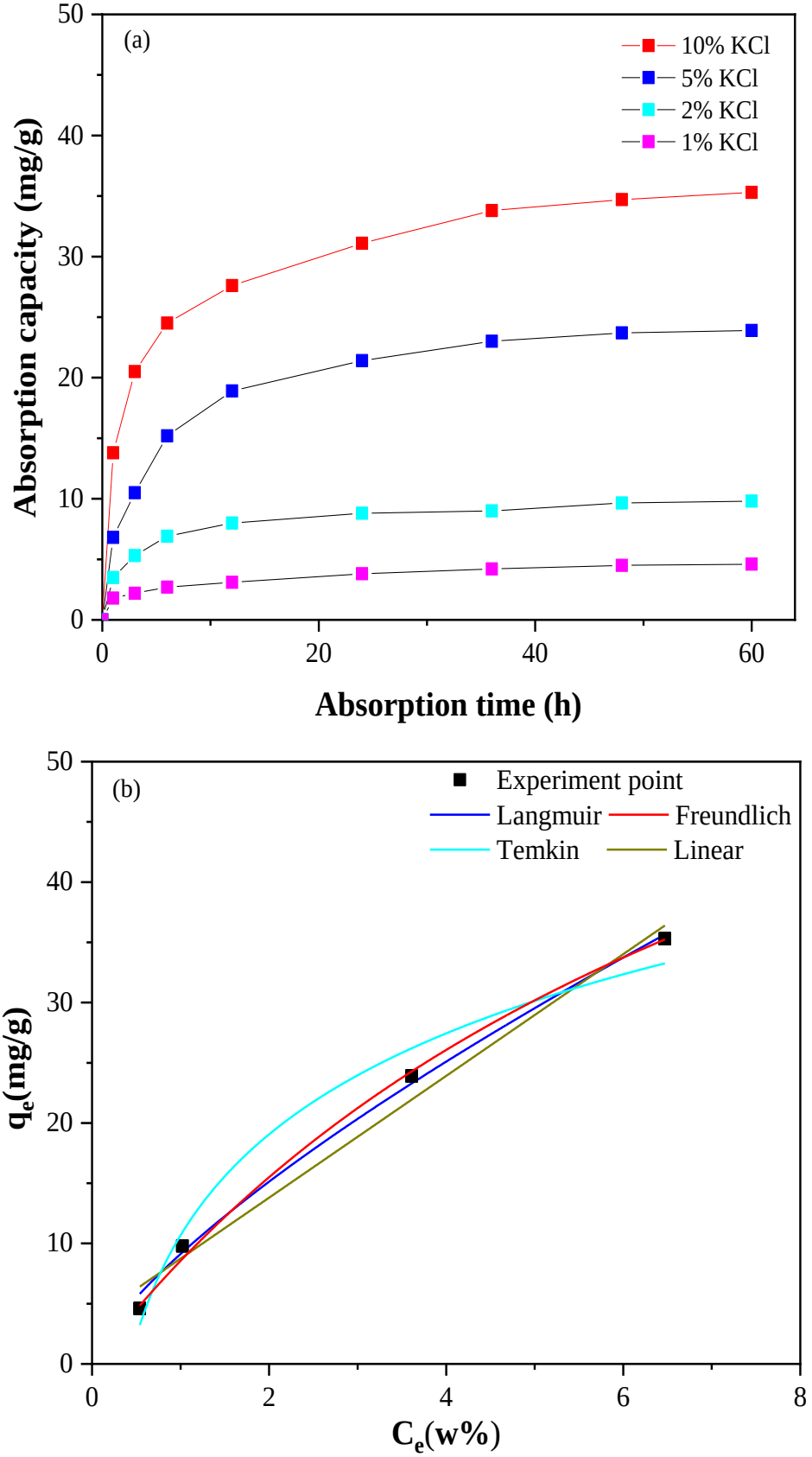

Figure 12. Adsorption curves of KCl: (**a**) absorption capacity over time and (**b**) adsorption isotherm.

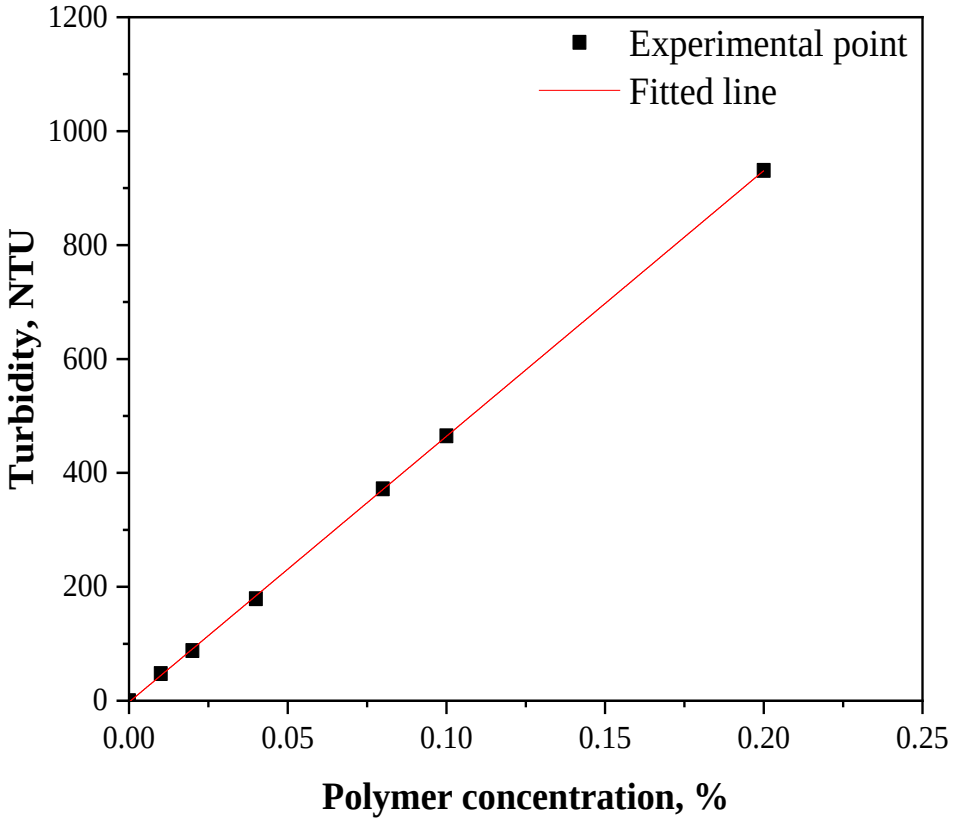

Figure 13. Standard curve diagram of polymer.

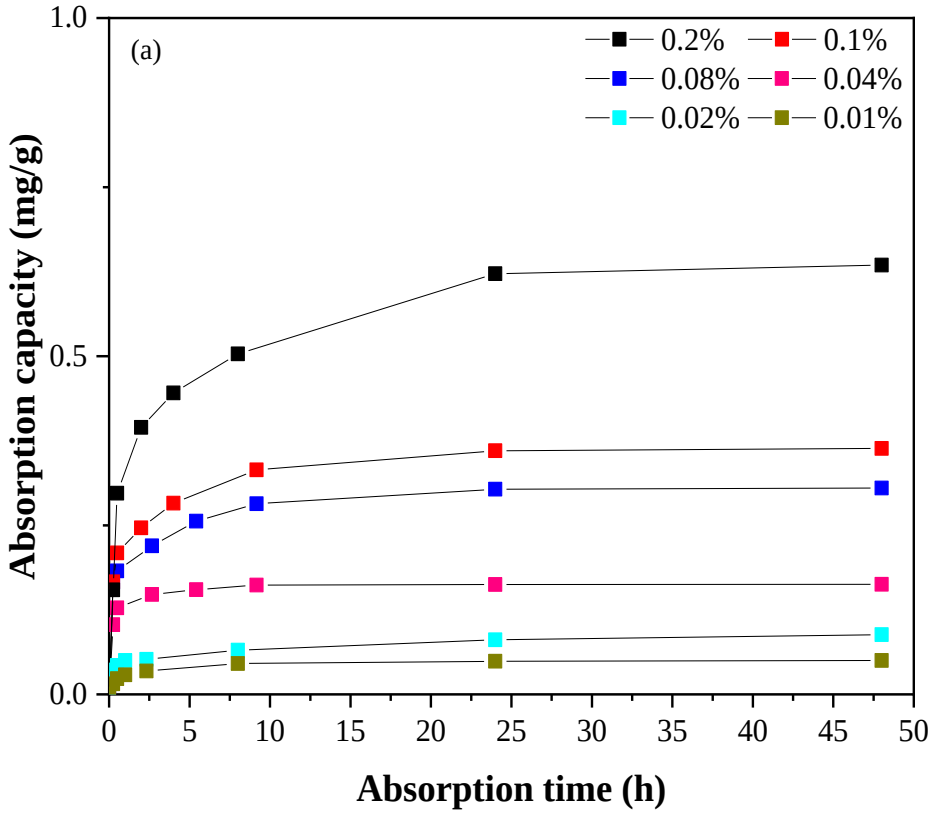

Figure 14. *Cont.*

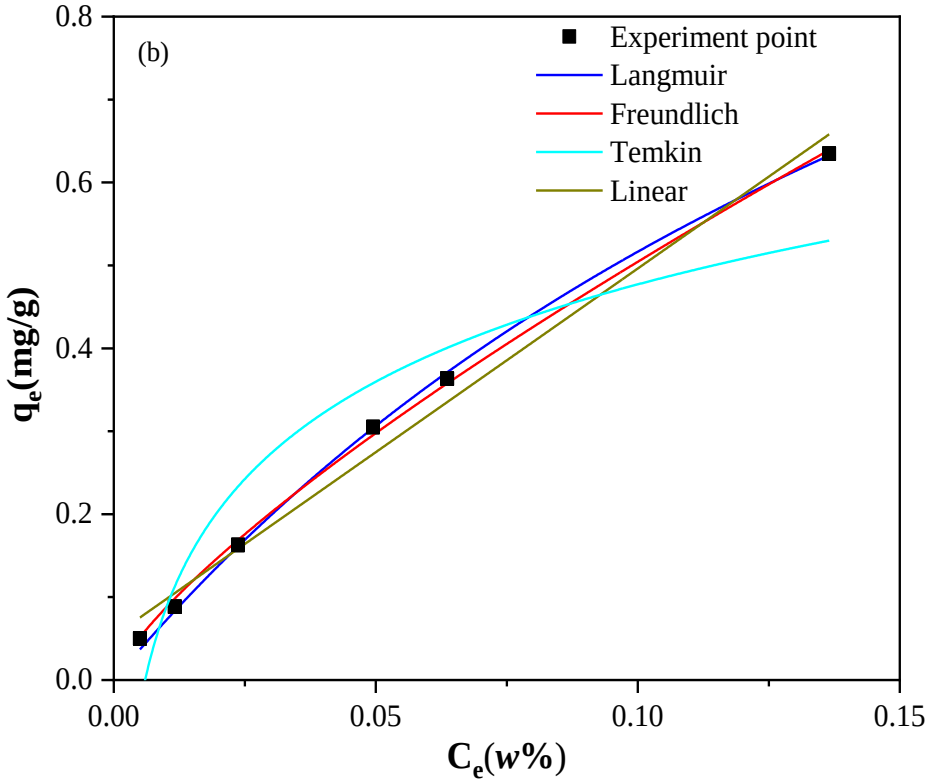

Figure 14. Adsorption curves of polymer: (**a**) adsorption capacity over time and (**b**) adsorption isotherm.

4. Conclusions

Variation in mineralization with respect to the fracture rejection fluid used in sandstone reservoirs over time are regarded as an essential tool for comprehending reservoirs and assessing the degree of artificial fracture network formation. However, the mechanisms of the low rejection rate and the high mineralization of the rejection fluid used in tight sandstone reservoirs are not well understood. In this work, we investigated the ion diffusion behavior of tight sandstone and its adsorption properties in fracturing fluid components. The main findings are summarized below:

(1) The tight sandstone reservoir has a 37.5% clay mineral concentration with an 8.74% linear swelling rate, resulting in moderately severe water–sensitive damage. Both potassium chloride and polyamide were effective in inhibiting the swelling of clay minerals; however, significantly more potassium chloride was added than polyamide.

(2) According to the results of low-temperature N_2 adsorption characterization, the structural parameters of tight sandstone nanopores changed significantly after adsorption when treated with different concentrations of KCl or polymer. The fractal dimension D_2 tended to increase with the increase in the polymer concentration. This indicates that polymer adsorption makes the pore throat structure of tight sandstone more complex and inhomogeneous, which is recognized as the main mechanism impairing permeability. However, the fractal dimension D_2 decreases with the increased mass fraction of KCl. It promotes a more uniform and consistent pore throat structure, which is an excellent behavior to improve the reservoir permeability.

(3) Self-imbibition of tight sandstone is always accompanied by ion diffusion phenomena. However, after the imbibition process stabilizes, the diffusion of salt ions proceeds, almost logarithmically, with time and takes a long time to reach stability. The diffusion rate of salt ions is controlled by the clay minerals and particle size. Pyrite is the most prominent source of ferrous ions in the flowback fluid, considerably increasing the conductivity of the solution. The high mineralization of fracturing rejection fluid can

be explained by the low pyrite content in tight sandstone and the large contribution of clay minerals to its conductivity.

(4) The absorption of both KCl and polymer on tight sandstone matches the Langmuir model; however, the adsorption mechanisms and their effects on the pore throat are very different. Potassium chloride adsorption increases the pore throat diameter of the rock and protects the permeability of the reservoir by increasing the pore throat's uniformity through electrostatic adsorption with clay minerals. However, the adsorption of polymers decreases the pore diameter of the rock and forms a thin film that obstructs the pore throat, complicating the pore throat and causing damage to its permeability.

Author Contributions: Conceptualization, X.Z. and Y.L. (Youquan Liu); methodology, Y.L. (Yuzhou Liu); validation, X.Z. and Y.L. (Youquan Liu); formal analysis, X.Z. and P.Z.; data curation, X.Z. and P.Z.; writing—original draft preparation, X.Z. and C.Z. All authors have read and agreed to the published version of the manuscript.

Funding: This work is supported financially by the postdoctoral research program of the Petrochina Southwest Oil & Gas Field Company (Grant No. 20220302-20).

Informed Consent Statement: Not applicable.

Data Availability Statement: Data presented in this study are available on request from the first author.

Conflicts of Interest: The authors declare no conflict of interest.

References

1. Alreshedan, F.; Kantzas, A. Investigation of permeability, formation factor, and porosity relationships for Mesaverde tight gas sandstones using random network models. *J. Pet. Explor. Prod. Technol.* **2016**, *6*, 545–554. [CrossRef]
2. Albrecht, D.; Reitenbach, V. Investigations on fluid transport properties in the North-German Rotliegend tight gas sandstones and applications. *Environ. Earth. Sci.* **2015**, *73*, 5791–5799. [CrossRef]
3. Dong, B.Q.; Meng, M.; Qiu, Z.S.; Lu, Z.H.; Zhang, Y.; Zhong, H.Y. Formation damage prevention using microemulsion in tight sandstone gas reservoir. *J. Pet. Sci. Eng.* **2019**, *173*, 101–111. [CrossRef]
4. Holditch, S.A. Tight gas sands. *J. Petrol. Technol.* **2006**, *58*, 86–93. [CrossRef]
5. Gao, H.; Li, H.A. Pore structure characterization, permeability evaluation and enhanced gas recovery techniques of tight gas sandstones. *J. Nat. Gas. Sci. Eng.* **2016**, *28*, 536–547. [CrossRef]
6. Yin, S.; Han, C.; Wu, Z.H.; Li, Q.M. Developmental characteristics, influencing factors and prediction of fractures for a tight gas sandstone in a gentle structural area of the Ordos Basin, China. *J. Nat. Gas. Sci. Eng.* **2019**, *72*, 103032. [CrossRef]
7. Tang, H.M.; Tang, H.X.; He, J.; Zhao, F.; Zhang, L.H.; Liao, J.J.; Wang, Q.; Yuan, X.F. Damage mechanism of water-based fracturing fluid to tight sandstone gas reservoirs: Improvement of The Evaluation Measurement for properties of Water-based Fracturing Fluid: SY/T 5107-2016. *Nat. Gas. Ind. B* **2021**, *8*, 163–172. [CrossRef]
8. Abaa, K.; Wang, J.; Elsworth, D.; Ityokumbul, M. Laboratory investigation of impact of slickwater composition on multiphase permeability evolution in tight sandstones. *SPE. Prod. Oper.* **2022**, *37*, 202–217. [CrossRef]
9. Zheng, Y.C.; Han, X.; Zeng, J.; Zhou, C.L.; Zhou, L.; Chen, W.H. Practice of high-intensity volume fracturing in the Shaximiao Formation tight sandstone gas reservoirs of the Qiulin Block, central Sichuan Basin. *Nat. Gas. Ind. B* **2021**, *8*, 367–375. [CrossRef]
10. Zhang, X.P.; Liu, Y.Q.; Liu, Y.Z.; Zhong, C.R. Influencing factors and application of spontaneous imbibition of fracturing fluids in tight sandstone gas reservoir. *ACS Omega* **2022**, *7*, 38912–38922. [CrossRef]
11. Sanyal, S.; Bhui, U.K.; Balaga, D.; Kumar, S.S. Interaction study of montmorillonite-crude oil-brine: Molecular-level implications on enhanced oil recovery during low saline water flooding from hydrocarbon reservoirs. *Fuel* **2019**, *254*, 115725. [CrossRef]
12. Mohan, K.K.; Fogler, H.S. Colloidally induced smectitic fines migration: Existence of microquakes. *AIChE J.* **1997**, *43*, 565–576. [CrossRef]
13. Johnston, K.; Martin, M.; Higginson, S. Case Study: Recharge of potable and tertiary treated wastewater into a deep confined sandstone aquifer in Perth, Western Australia. In *Clogging Issues Associated with Managed Aquifer Recharge Methods*; IAH: London, UK, 2013; pp. 174–183.
14. Barnaji, M.J.; Pourafshary, P.; Rasaie, M.R. Visual investigation of the effects of clay minerals on enhancement of oil recovery by low salinity water flooding. *Fuel* **2016**, *184*, 826–835. [CrossRef]
15. Olsson, O.; Weichgrebe, D.; Rosenwinkel, K.H. Hydraulic fracturing wastewater in Germany: Composition, treatment, concerns. *Environ. Earth. Sci.* **2013**, *70*, 3895–3906. [CrossRef]
16. Tian, J.; Qin, C.; Kang, Y.; You, L.; Jia, N.; Song, J. Reasons for low flowback behaviors of water-based fluids in tight sandstone gas reservoirs. *J. Pet. Sci. Eng.* **2022**, *220*, 111152. [CrossRef]

17. Mao, J.C.; Zhang, C.; Yang, X.J.; Zhang, Z.Y. Investigation on problems of wastewater from hydraulic fracturing and their solutions. *Water. Air. Soil. Pollut.* **2018**, *229*, 1–13. [CrossRef]
18. Yang, L.; Chen, C.J.; Liu, Y.F.; Zheng, Y.H. A comparative study of ion diffusion during water imbibition in shale, sandstone and volcanic rock. *Capillarity* **2020**, *3*, 16–27. [CrossRef]
19. Zolfaghari, A.; Dehghanpour, H.; Ghanbari, E.; Bearinger, D. Fracture characterization using flowback salt-concentration transient. *SPE J.* **2016**, *21*, 233–244. [CrossRef]
20. Meng, M.M.; Ge, H.K.; Shen, Y.H.; Wang, L.L. Influence of rock fabric on salt ion diffusion behavior in upper cretaceous lacustrine shale from Songliao Basin. *J. Pet. Sci. Eng.* **2022**, *208*, 109355. [CrossRef]
21. Zhong, H.Y.; Huang, W.A.; Qiu, Z.S.; Huang, D.Q.; Wang, F.W. Experimental study of the scale inhibition between polyamine and potassium chloride. *J. Southw. Petroleum Univ. (Nat. Sci. Ed.)* **2012**, *34*, 151–156. (In Chinese)
22. Maia, A.M.S.; Borsali, R.; Balaban, R.C. Comparison between a polyacrylamide and a hydrophobically modified polyacrylamide flood in a sandstone core. *Mat. Sci. Eng. C* **2009**, *29*, 505–509. [CrossRef]
23. Abrahmsén-Alami, S.; Alami, E.; François, J. The lyotropic cubic phase of model associative polymers: Small-angle X-ray scattering (SAXS), differential scanning calorimetry (DSC), and turbidity measurements. *J. Colloid. Interf. Sci.* **1996**, *179*, 20–33. [CrossRef]
24. Langmuir, I. The constitution and fundamental properties of solids and liquids. II. Liquids. *J. Am. Chem. Soc.* **1917**, *39*, 1848–1906. [CrossRef]
25. Freundlich, H.M.F. Über die Adsorptiontion in Lösungen. *Z. Phys. Chem.* **1906**, *57*, 387–470.
26. Tempkin, M.J.; Pyzhev, V. Recent modifications to Langmuir isotherms. *Acta Physiochim. USSR* **1940**, *12*, 217–222.
27. Lagergren, S. Zur theorie der sogenannten adsorption geloster stoffe. Kungliga svenska vetenskapsakademiens. *Handlingar.* **1898**, *24*, 1–39.
28. Mandelbrot, B.B. On the geometry of homogeneous turbulence, with stress on the fractal dimension of the iso-surfaces of scalars. *J. Fluid. Mech.* **1975**, *72*, 401–416. [CrossRef]
29. Pfeifer, P.; Avnir, D. Chemistry in noninteger dimensions between two and three: Fractal theory of herrgeneous surface. *J. Chem. Phys.* **1983**, *79*, 3558–3565. [CrossRef]
30. Krohn, C.E. Fractal measurements of sandstones, shales, and carbonates. *J. Geophys. Res. Atmos.* **1988**, *93*, 3297–3305. [CrossRef]
31. Zhao, X.; Yang, Z.; Lin, W.; Xiong, S.; Luo, Y.; Wang, Z.; Chen, T.; Xia, D.; Wu, Z. Study on pore structures of tight sandstone reservoirs based on nitrogen adsorption, high-pressure mercury intrusion, and rate-controlled mercury intrusion. *J. Energy Resour. Technol.* **2019**, *141*, 112903. [CrossRef]
32. Li, X.H.; Gao, Z.Y.; Fang, S.Y.; Ren, C.; Yang, K.; Wang, F.Y. Fractal characterization of nanopore structure in shale, tight sandstone and mudstone from the Ordos basin of China using nitrogen adsorption. *Energies* **2019**, *12*, 583. [CrossRef]
33. Wang, F.Y.; Yang, K.; You, J.X.; Lei, X.J. Analysis of pore size distribution and fractal dimension in tight sandstone with mercury intrusion porosimetry. *Results Phys.* **2019**, *13*, 102283. [CrossRef]
34. Wang, F.Y.; Yang, K.; Zai, Y. Multifractal characteristics of shale and tight sandstone pore structures with nitrogen adsorption and nuclear magnetic resonance. *Pet. Sci.* **2020**, *17*, 1209–1220. [CrossRef]
35. Shao, X.; Pang, X.; Li, H.; Zhang, X. Fractal analysis of pore network in tight gas sandstones using NMR method: A case study from the Ordos Basin, China. *Energy Fuels* **2017**, *31*, 10358–10368. [CrossRef]
36. Sikiru, S. Ionic transport and influence of electromagnetic field interaction within electric double layer in reservoir sandstone. *J. Mol. Liq.* **2021**, *344*, 117675. [CrossRef]